

# UC Berkeley

## UC Berkeley Previously Published Works

### Title

Ruthenium-Catalyzed Hydroamination of Unactivated Terminal Alkenes with Stoichiometric Amounts of Alkene and an Ammonia Surrogate by Sequential Oxidation and Reduction

### Permalink

<https://escholarship.org/uc/item/5zt4d7zw>

### Journal

Journal of the American Chemical Society, 143(1)

### ISSN

0002-7863

### Authors

Ma, Senjie  
Hill, Christopher K  
Olen, Casey L  
[et al.](#)

### Publication Date

2021-01-13

### DOI

10.1021/jacs.0c11043

Peer reviewed



# HHS Public Access

Author manuscript

*J Am Chem Soc.* Author manuscript; available in PMC 2021 November 16.

Published in final edited form as:

*J Am Chem Soc.* 2021 January 13; 143(1): 359–368. doi:10.1021/jacs.0c11043.

## Ruthenium-Catalyzed Hydroamination of Unactivated Terminal Alkenes with Stoichiometric Amounts of Alkene and an Ammonia Surrogate by Sequential Oxidation and Reduction

**Senjie Ma,**

Department of Chemistry, University of California, Berkeley, California 94720, United States;

**Christopher K. Hill,**

Department of Chemistry, University of California, Berkeley, California 94720, United States;

**Casey L. Olen,**

Department of Chemistry, University of California, Berkeley, California 94720, United States;

**John F. Hartwig**

Department of Chemistry, University of California, Berkeley, California 94720, United States;

### Abstract

Hydroamination of alkenes catalyzed by transition-metal complexes is an atom-economical method for the synthesis of amines, but reactions of unactivated alkenes remain inefficient. Additions of N–H bonds to such alkenes catalyzed by iridium, gold, and lanthanide catalysts are known, but they have required a large excess of the alkene. New mechanisms for such processes involving metals rarely used previously for hydroamination could enable these reactions to occur with greater efficiency. We report ruthenium-catalyzed intermolecular hydroaminations of a variety of unactivated terminal alkenes without the need for an excess of alkene and with 2-aminopyridine as an ammonia surrogate to give the Markovnikov addition product. Ruthenium complexes have rarely been used for hydroaminations and have not previously catalyzed such reactions with unactivated alkenes. Identification of the catalyst resting state, kinetic measurements, deuterium labeling studies, and DFT computations were conducted and, together, strongly suggest that this process occurs by a new mechanism for hydroamination occurring by oxidative amination in concert with reduction of the resulting imine.

### Graphical Abstract

**Corresponding Author: John F. Hartwig** – Department of Chemistry, University of California, Berkeley, California 94720, United States; jhartwig@berkeley.edu.

Supporting Information

The Supporting Information is available free of charge at <https://pubs.acs.org/doi/10.1021/jacs.0c11043>.

Experimental procedures, characterization of new compounds, information about computational studies, and crystallographic information (PDF)

X-ray crystallographic data for Ru(PEt<sub>3</sub>)<sub>3</sub>(NTf<sub>2</sub>)<sub>2</sub> (CIF)

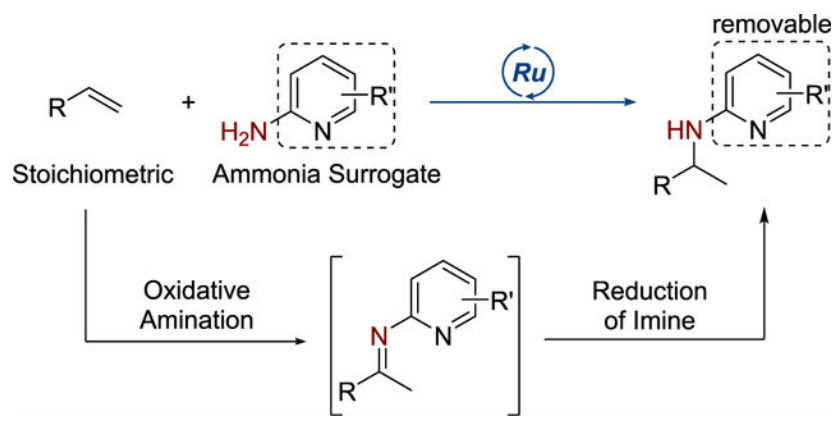
X-ray crystallographic data for Ru(PEt<sub>3</sub>)<sub>3</sub>(amine)-(NTf<sub>2</sub>)<sub>2</sub> (29) (CIF)

X-ray crystallographic data for Ru(PEt<sub>3</sub>)<sub>3</sub>(amido)(NTf<sub>2</sub>) (30) (CIF)

X-ray crystallographic data for Ru(H)(PEt<sub>3</sub>)<sub>3</sub>(amine)-(NTf<sub>2</sub>)<sub>2</sub> (44) (CIF)

Complete contact information is available at: <https://pubs.acs.org/10.1021/jacs.0c11043>

The authors declare no competing financial interest.



## INTRODUCTION

Amines and their derivatives are important as both pharmaceuticals and agrochemicals.<sup>1–3</sup> Traditional methods to synthesize amines include nucleophilic substitution of organic halides,<sup>4</sup> reductive amination of carbonyl compounds,<sup>5</sup> and reduction of amides, nitriles, and azides.<sup>6</sup> The hydroamination of alkenes catalyzed by transition-metal complexes is an attractive alternative to these methods because it occurs directly with alkenes and could be applied to the functionalization of both simple alkenes and complex molecules containing alkene units.<sup>7–9</sup> Despite the potential utility of hydroamination, examples of intermolecular hydroaminations are often limited to conjugated and strained alkenes, such as dienes,<sup>10,11</sup> vinylarenes,<sup>12,13</sup> norbornenes,<sup>14,15</sup> and cyclopropenes.<sup>16,17</sup> Hydroaminations of unactivated alkenes are rare and generally require a large excess of alkene (Scheme 1a).<sup>18–26</sup>

Two main strategies have been followed to enable hydroamination to occur without an excess amount of alkene. The first involves catalytic reactions of alkenes possessing a directing group (Scheme 1b);<sup>27,28</sup> the second involves a formal catalytic hydroamination achieved by combining a silane reducing agent and a nitrogen-based electrophile (Scheme 1c).<sup>29,30</sup> These strategies require special alkenes or generate stoichiometric amounts of waste from the silane and aminating reagents and require synthesis of the aminating reagent. Thus, the development of a method that involves the direct addition of the N–H bond of an amine to unactivated alkenes is needed and would address these drawbacks.

Two general classes of mechanisms have been followed by most late, transition-metal catalysts for the hydroamination of alkenes. The first mechanism involves nucleophilic attack of a nitrogen nucleophile on a coordinated alkene, followed by protonation of the resulting amino-alkyl intermediate. The second involves oxidative addition of an N–H bond, followed by migratory insertion of the alkene into the metal–nitrogen bond and reductive elimination to form the C–H bond. Cationic rhodium<sup>31</sup> and gold<sup>22</sup> systems react by the first pathway, whereas neutral iridium complexes<sup>19</sup> react by the second pathway. Ruthenium complexes, the subject of this work, catalyze the hydroamination of terminal alkynes<sup>32</sup> and vinylarenes,<sup>13</sup> but they have not been shown to catalyze the hydroamination of unconjugated alkenes. We considered that such complexes and a carefully designed amine could catalyze

the hydroaminations of alkenes and do so by mechanisms that are distinct from those followed by complexes of other transition metals.

Multidentate coordination of an amine that is tethered to a Lewis basic group, rather than an alkene tethered to such a group, can accelerate hydroaminations due to a series of effects. First, the Lewis basic group can stabilize the intermediates resulting from oxidative addition of the N–H bond and products from insertion. Second, such an amine can serve as an ammonia equivalent by removal of the Lewis basic group. Third, an appropriate heteroaryl substituent can alter the thermodynamics of this nearly thermoneutral process<sup>33</sup> to favor addition by rendering the N–H bond of the ammonia surrogate weaker than the N–H bond of ammonia.

We report ruthenium-catalyzed Markovnikov hydroaminations of unactivated, terminal alkenes with 2-aminopyridine as an ammonia surrogate (Scheme 1d). Terminal alkenes containing a series of functional groups undergo hydroamination in the presence of this catalyst to afford the corresponding amine products without excess alkene. Detailed experimental and computational mechanistic studies provide strong evidence that this reaction occurs by a new pathway for hydroamination that comprises oxidative amination of the alkene and reduction of the corresponding imine intermediate.

## RESULTS AND DISCUSSION

### Reaction Development.

Our studies on ruthenium-catalyzed hydroamination of unactivated terminal alkenes began by examining the reaction between 1-dodecene (1.0 equiv) and 2-aminopyridine **1a** (1.0 equiv) in the presence of a variety of electrophilic ruthenium complexes, a class of catalyst previously reported by our group to catalyze the oxidation of alcohols<sup>34</sup> (Table 1). 2-Aminopyridine was investigated as the amine component because it could coordinate to the cationic ruthenium complex in a bidentate fashion to form a four-membered ruthenacycle that would retain reactivity at the Ru–N bond, due to the ring strain.

A survey of a series of phosphine-ligated ruthenium triflimide and triflate complexes showed that the triethylphosphine-ligated ruthenium complex **Ru-1** containing triflimide as the anionic ligand catalyzes the hydroamination of 1-dodecene to afford the amine product **2a** in 67% yield (Table 1, entry 1). Entries 2–6 show the effect of the phosphine ligand. Ruthenium complexes that contain more sterically demanding phosphine ligands (entry 2) and less electron-rich phosphine ligands (entry 3) catalyzed the reactions to form the addition product in lower yields. Complexes of ruthenium ligated by trimethylphosphine, 1,2-bis(diethylphosphino)-butane, and a tripodal phosphine ligand, N(CH<sub>2</sub>PEt<sub>2</sub>)<sub>3</sub>, did not catalyze the hydroamination reaction (entries 4–6). Entries 7 and 8 show the effect of the anionic ligand. Hydroamination conducted with the PEt<sub>3</sub>-ligated ruthenium complex containing triflate counteranion (**Ru-7**) afforded the product in a slightly lower 62% yield (entry 7) than that with **Ru-1**, and the PEt<sub>3</sub>-ligated ruthenium complex containing chlorides (**Ru-8**) did not catalyze the hydroamination reaction (entry 8). This hydroamination proceeded in a variety of polar, noncoordinating solvents, and the reaction in 1,2-DCB (entry 1) occurred in a higher yield than did reactions in other solvents of this class (entries

9–14). The reaction performed with 2 mol % of **Ru-1** instead of 5 mol % gave a lower yield of product (entry 15).

Hydroaminations of alkenes catalyzed by electrophilic metal complexes, in some cases, have been suspected to occur by acid generated from the amine and the complex.<sup>35</sup> Although the basicity of the 2-aminopyridine would render such a pathway unlikely, we conducted control experiments to test this potential. To assess the role of the ruthenium complex in this reaction, we conducted the reaction in the absence of **Ru-1**. Without **Ru-1**, no detectable product formed, indicating that the ruthenium complex is necessary for this transformation (entry 16). The hydroamination of 1-dodecene with substoichiometric amounts of strong acid also did not form detectable amounts of product (entry 17), providing evidence against a pathway for hydroamination with 2-aminopyridine catalyzed by a Brønsted acid.

### Scope of Terminal Alkenes and 2-Aminopyridines for Catalytic Hydroamination.

Studies on the scope of the ruthenium-catalyzed hydroamination under the developed conditions are summarized in Table 2. The hydroamination of terminal alkenes with alkyl and aryl substituents occurred to afford products in good yields (**2a–4a**). The hydroamination of a series of alkenes bearing ether, fluoride, amide, and tertiary alcohol functional groups also formed the hydroamination products in good to moderate yields (**5a–8a**). Alkenes containing multiple double bonds underwent hydroamination exclusively at the terminal alkene (**9a–11a**). Even the hydroamination of boldenone undecylenate, an anabolic steroid, occurred, showing the potential of this methodology for late-stage functionalization of architecturally complex molecules containing potential competing functionality (**12a**). An investigation of the scope of 2-aminopyridines for this reaction showed that a variety of 2-aminopyridines containing alkyl, ether, sulfide, and methylpiperazine substituents reacted to give the hydroamination products (**13a–17a**).

In addition to unconjugated, terminal alkenes, vinylarenes underwent this hydroamination reaction (Table 3). Vinylarenes bearing a variety of electron-donating and electron-withdrawing *para*-substituents underwent hydroamination to afford products in good yields (**18a–24a**). However, higher temperatures were required for the hydroaminations of electron-deficient vinylarenes catalyzed by **Ru-1** (**20a, 22–24a**). A lower yield was observed from the reaction of a vinylarene bearing an *ortho*-substituent (**25a**), indicating that the reaction is sensitive to steric hindrance. The hydroamination of vinylnaphthalene and vinylferrocene also proceeded to afford hydroamination products (**27a–28a**). The major side reaction observed during the hydroamination was the isomerization of the terminal alkene to form internal alkenes, which did not undergo hydroamination under our reaction conditions. High yields of the amine products **2a, 8a, 12a, 16a, and 28a** were obtained for reactions with just 2 equiv of alkene with respect to the aminopyridine.

### Removal of Pyridyl Group from the Hydroamination Product.

The product from the hydroamination reaction was converted to a primary amine by a two-step sequence (Scheme 2).<sup>36–38</sup> Compound **2a** was first converted to an amidine, and the amidine was cleaved by NaBH<sub>4</sub> to form primary amine **2b**. For convenience on the laboratory scale, the Boc-protected amine **2c** was isolated instead of the free amine **2b**.

## Mechanistic Studies of Alkene Hydroamination.

Because side reactions, such as alkene isomerization, alkene oligomerization, and oxidative amination, compete with alkene hydroamination,<sup>9,19,39</sup> literature protocols for the hydroamination of unactivated alkenes require either the use of alkenes containing a directing group or excess alkene. Our hydroamination protocol represents a rare example of catalytic hydroamination of unactivated alkenes with a stoichiometric amount of alkene. Therefore, a detailed investigation of the mechanism of this ruthenium-catalyzed hydroamination reaction was conducted to provide insight into the features that promote the hydroamination reaction over other side reactions.

## Determination of the Catalyst Resting State.

Our mechanistic investigation began with identifying the catalyst resting state. To obtain preliminary information about this species, we monitored the reaction of 2-amino-4-methylpyridine (**1b**) and 1-dodecene catalyzed by **Ru-1** by <sup>31</sup>P NMR spectroscopy at 80 °C (spectrum b of Figure 1). Aminopyridine **1b** was used for these studies, instead of **1a**, because ruthenium complexes containing **1b** were more crystalline than those containing **1a** (vide infra). A broad resonance at 50 ppm, corresponding to the resting state of the catalyst, was observed in the <sup>31</sup>P NMR spectrum of the reaction mixture.

Further information on the identity of the resting state was obtained by allowing **Ru-1** to react with 1-dodecene and **1b** separately and monitoring the reaction mixtures by <sup>31</sup>P NMR spectroscopy. Treatment of **Ru-1** with excess 1-dodecene led to no new Ru complexes, as determined by <sup>31</sup>P NMR spectroscopy at 80 °C (a and c of Figure 1). However, treatment of **Ru-1** with excess aminopyridine **1b** led to the observation of a broad resonance at 50 ppm in the <sup>31</sup>P NMR spectrum of the reaction mixture at 80 °C, and this resonance was identical to that of the resting state of the Ru catalyst (d of Figure 1). Therefore, the major ruthenium complex in the reaction system forms from the combination of **Ru-1** with one or more equiv of aminopyridine **1b**.

An independent synthesis of the resting state was pursued (Figure 2) because we were unable to isolate it in pure form directly from the mixture of **Ru-1** and excess **1b**. Treatment of **Ru-1** with 1 equiv of **1b** afforded the aminopyridine-coordinated ruthenium complex **29** in 82% yield after recrystallization (Figure 2a). The <sup>31</sup>P NMR spectrum of complex **29** contained a single <sup>31</sup>P resonance at 38 ppm, and the structure of **29** was determined by single-crystal X-ray diffraction. The Ru center in **29** is ligated by three PEt<sub>3</sub> ligands, one *O*-bound triflimide, and one  $\kappa^2$ -bound aminopyridine in an octahedral geometry (Figure 2c). The <sup>31</sup>P NMR chemical shift of 38 ppm for complex **29** is distinct from that of the catalyst resting state (50 ppm).

Thus, we postulated that coordination of **1b** to the cationic ruthenium center sufficiently acidifies the N–H bonds to cause deprotonation of **29** by another equivalent of aminopyridine. To test this hypothesis, we treated complex **29** with an insoluble base (K<sub>3</sub>PO<sub>4</sub>). This reaction led to the isolation of the Ru–amido complex **30** in 85% yield after recrystallization (Figure 2b). The <sup>31</sup>P NMR spectrum of complex **30** consisted of a single sharp resonance at 51 ppm (e of Figure 1). The solid-state structure of complex **30**

was determined by X-ray diffraction (Figure 2d). This complex adopts a square pyramidal geometry with an empty coordination site trans to a  $\text{PEt}_3$  ligand.

The hydroamination of 1-dodecene by aminopyridine **1b** catalyzed by 5 mol % of the isolated complex **30** afforded the product **13a** in 65% yield in 48 h. This result indicates that complex **30** is kinetically competent to be an intermediate in this hydroamination reaction. Furthermore, a broad resonance at 50 ppm, which matched that observed for the catalytic reaction initiated with **Ru-1**, was observed in the  $^{31}\text{P}$  NMR spectrum of the hydroamination reaction initiated with complex **30** as catalyst (f of Figure 1).

These data suggest that complex **30** could be the resting state of the catalyst, but the resonance corresponding to isolated **30** is much sharper and slightly more downfield (0.9 ppm) than that of the major ruthenium complex in the catalytic system. We determined that this difference in line shape and chemical shift depends on the presence or absence of an excess of the aminopyridine; the  $^{31}\text{P}$  NMR signal of isolated **30** broadened and shifted slightly upfield in the presence of 20 equiv of aminopyridine **1b** at 80 °C (g of Figure 1).

To investigate the origin of this difference in line shape and chemical shift further, we conducted variable-temperature NMR spectroscopy with a 20:1 mixture of aminopyridine **1b** and complex **30** (Figure 3). At -40 °C, the  $^{31}\text{P}$  NMR spectrum of the mixture contained three triplet resonances. A potential structure for the complex corresponding to the three triplet resonances is **31a** shown at the bottom of Figure 3. This structure contains an additional 2-aminopyridine occupying the sixth coordination site and a hydrogen bond to the amido ligand. The hydrogen-bonding interaction in **31a** is evidenced by the observation of a broad downfield proton resonance (14 ppm) in the  $^1\text{H}$  NMR spectrum of this mixture. The integration of the three triplet resonances in the  $^{31}\text{P}$  NMR spectrum decreased at higher temperatures, and we were unable to detect the triple resonances when the temperature of the mixture reached 40 °C, indicating that complex **31a** is a minor species in the catalytic reaction at 80 °C.

The chemical shift of the broad resonance corresponding to the major ruthenium complex at 80 °C migrated significantly upfield at lower temperature. The origin of this line shape and change in chemical shift is not clear, but could result from hydrogen bonding between the amide ligand NH and the aminopyridine without coordination of the pyridine nitrogen to the metal as we suggest is present in complex **31b**. The chemical shift of this resonance lies further upfield in solutions containing higher concentrations of aminopyridine, implying that the resonance results from an equilibrium between **30** and an adduct formed between **30** and the aminopyridine that is distinct from complex **31a**. At the same time, the similarity in chemical shift between pure complex **30** and the resonance in the presence of aminopyridine at the concentration and 80 °C temperature of the reaction implies that the major component in the catalytic reaction is complex **30**.

### Kinetic Studies on Catalytic Hydroamination.

Kinetic experiments were conducted to gain further information on the mechanism of the hydroamination. Kinetic experiments with 1-dodecene as the substrate were complicated by



the observation of alkene isomerization during the reaction. Therefore, we conducted kinetic studies with vinylcyclohexane, which did not undergo competing isomerization.

Initial rates of the hydroamination reaction were measured at a series of concentrations of vinylcyclohexane, aminopyridine **1b**, and catalyst **Ru-1** (see the Supporting Information for details). Plots of initial rates against the concentration of the vinylcyclohexane, **1b**, and **Ru-1** are shown in Figure 4a–c. We found that the hydroamination reaction is first order in the concentration of vinylcyclohexane, zero order in the concentration of **1b**, and first order in the concentration of **Ru-1**. The orders in alkene and catalyst imply that these species react in the turnover-limiting step. The zero-order dependence of the reaction on the concentration of aminopyridine **1b** suggests that the hydroamination does not proceed by turnover-limiting nucleophilic attack of **1b** on the alkene in a Ru complex like **32** (Scheme 3, pathway a). Instead, the kinetic data are consistent with a migratory insertion of the alkene into the Ru–N bond of the Ru–alkene complex **32** to generate a Ru–alkyl complex **33** (Scheme 3, pathway b).

The effect of the concentration of  $\text{PEt}_3$  on the rate of the catalytic hydroamination was also studied. Added  $\text{PEt}_3$  inhibited the reaction, and a plot of  $1/\text{initial rate}$  against the concentration of  $\text{PEt}_3$  was linear (Figure 4d). To account for this observation, we considered two hypotheses. First, the added  $\text{PEt}_3$  could inhibit the reaction by reversibly coordinating to complex **30** to generate complex **34** (Scheme 4a). Second, reversible dissociation of  $\text{PEt}_3$  from complex **30** could generate the catalytically active complex **35** (Scheme 4b). To test these hypotheses, variable-temperature NMR spectroscopy analysis was conducted with a 5:1 mixture of  $\text{PEt}_3$  and complex **30**. Full conversion of **30** to complex **34** was observed by  $^{31}\text{P}$  NMR spectroscopy of this mixture at  $-20\text{ }^\circ\text{C}$  (see the Supporting Information for details). In addition, the association of  $\text{PEt}_3$  to complex **30** was computed by DFT to be exergonic by 0.3 kcal/mol at  $-20\text{ }^\circ\text{C}$ , whereas the dissociation of  $\text{PEt}_3$  from complex **30** was calculated to be endergonic by an energy (31.5 kcal/mol at  $80\text{ }^\circ\text{C}$ ) that exceeds the entire 30.5 kcal/mol barrier for the reaction determined from the experimental rates. Therefore, we conclude that the origin of the inhibition of the hydroamination by added  $\text{PEt}_3$  results from the reversible coordination of  $\text{PEt}_3$  to complex **30** to form the inactive tetraphosphine complex **34** (Scheme 4a).

### Studies on the Pathway for the Formation of the Product from Ru–Alkyl Complex **33**.

To elucidate the pathway by which the product of this hydroamination reaction was formed from the Ru–alkyl complex **33**, the hydroamination of vinylcyclohexane was performed with **1b- $d_2$**  under the standard catalytic conditions (Table 4). Deuterium incorporation was observed at four different positions in the product **17a- $d_n$** . The ratios of the percentage of deuterium incorporation at the  $\text{H}_a$  and  $\text{H}_b$  positions were 1:1 at various time points during the reaction (Table 4), and the accumulation of deuterium into the starting vinylcyclohexane was not observed.

The results of this labeling study are consistent with the pathway in Scheme 5. By this pathway, coordination and migratory insertion of the alkene occur to form Ru–alkyl complex **33- $d$**  from the catalyst resting state **30- $d$** , after which complex **33- $d$**  undergoes a subsequent



$\beta$ -hydride elimination to generate the ruthenium–hydride species **44** ([Ru–H]) (Figure 5a) and enamine **36-d**. The enamine **36-d** would then undergo tautomerization catalyzed by protonated aminopyridine, which was formed during the generation of the catalyst resting state **30-d**. This tautomerization forms the  $\beta$ -deuterated imine **37-d**. Intramolecular H–D exchange between the Ru–H position and bound aminopyridine in complex **44** would generate a ruthenium–deuteride. Subsequent reduction of imine **37-d** by complex **44** containing a Ru–D bond would generate the final hydroamination product **17a-d<sub>n</sub>**, containing an enhanced level of deuterium at the H <sub>$\alpha$</sub>  and H <sub>$\beta$</sub>  positions. Because the tautomerization step and H/D exchange of the hydride position of complex **44** occur by reversible proton transfers involving the amino group in **1b**, the amounts of deuterium in the H <sub>$\alpha$</sub>  and H <sub>$\beta$</sub>  positions of the product are equal to each other. Furthermore, the observation of the incorporation of deuterium at the  $\alpha$  position of the product **17a-d<sub>n</sub>** provides evidence against a nucleophilic attack of **1b** on the metal-bound alkene complex, like **32** (Scheme 3, pathway a), because the coordinative saturation of the complex formed after a nucleophilic attack of the aminopyridine would disfavor  $\beta$ -hydrogen elimination.

To investigate the pathway for the formation of the hydroamination product further, we conducted the hydroamination of 1-dodecene with **1b** in the presence of 1 equiv of acetone. 2-Dodecanone **38** and the product from reductive amination of acetone **39** were observed, along with the hydroamination product **13a** (Scheme 6). The formation of **38** and **39** implies that the reaction occurs through an imine intermediate. Dodecyl enamine **40** is generated by migratory insertion of the alkene into the amidopyridine complex **30** and  $\beta$ -hydride elimination from metallacycle **33**. A subsequent tautomerization of the enamine **40** forms dodecyl imine **42**. Isopropyl imine **41** and water are generated by reversible condensation of acetone with aminopyridine **1b**. The imines **41** and **42** undergo competitive reduction to yield amines **13a** and **39**, respectively. The portion of imine **42** that is not reduced is hydrolyzed to give ketone **38**, which is detected by <sup>1</sup>H NMR spectroscopy.

To elucidate the identity of the proposed [Ru–H] intermediate that would result from  $\beta$ -H elimination of the aminoalkyl intermediate, we exposed complex **30** to 1 atm of H<sub>2</sub> (Figure 5a). Complex **43**, which resulted from the overall addition of H<sub>2</sub> across the Ru–N bond of complex **30** and coordination of H<sub>2</sub>, was observed. The structure of this complex was deduced by the observation of two distinct ruthenium hydride signals in the <sup>1</sup>H NMR spectrum. The H<sub>2</sub> ligand in **43** was slowly replaced by N<sub>2</sub> in a nitrogen atmosphere to afford complex **44**, which was characterized by single-crystal X-ray diffraction (Figure 5a,b).

Under an atmosphere of H<sub>2</sub>, the imine generated in situ from ketone **38** and aminopyridine **1b** underwent hydrogenation to form amine **13a** catalyzed by the amido complex **30** in 95% yield (Figure 5c). This result indicates that the hydridoruthenium complex **43** that would form in situ during the catalytic process from complex **30** and H<sub>2</sub> catalyzes the reduction of imines, such as **41** that would be formed in the catalytic process, to generate the final amine **13a**.

## DFT Computational Studies of the Proposed Catalytic Cycle for the Ruthenium-Catalyzed Hydroamination of Terminal Alkenes.

Our mechanistic experiments imply that this Ru-catalyzed hydroamination of terminal alkenes with 2-aminopyridine occurs by coordination of alkene to the catalyst resting state **30**, followed by migratory insertion of the alkene into the Ru–N bond,  $\beta$ -hydride elimination to generate an enamine, tautomerization of the enamine to an imine, and reduction of the imine to afford to amine product. Our kinetic studies indicate that the alkene and the ruthenium catalyst are involved in the turnover-limiting step. Hydrogenation of the imine cannot be turnover limiting because this step occurs faster than the overall hydroamination of the alkene (Figure 5c). To determine whether migratory insertion or  $\beta$ -hydride elimination following a reversible insertion process is turnover-limiting, DFT computations were conducted on the oxidative amination portion of the mechanism.

This mechanism was calculated for the hydroamination of propene, as a model alkene, with aminopyridine **1b**. An energy diagram for this process is shown in Figure 6. The coordination of propene to the catalyst resting state **30** was calculated to be endergonic at 16.2 kcal/mol. The free-energy barrier to the elementary migratory insertion of propene into the Ru–N bond was computed to be 12.5 kcal/mol (**32** to **TS1**). These energies lead to an overall barrier for coordination and insertion of 28.7 kcal/mol. The metallacycle **33** formed from insertion was computed to lie 8.1 kcal/mol uphill of the starting complex and free propene, and the barrier for  $\beta$ -hydride elimination from complex **33** was computed to be 11.2 kcal/mol (**33** to **TS2**). Thus, the transition state for the  $\beta$ -hydride elimination lies 19.3 kcal/mol uphill of the starting species and nearly 10 kcal/mol below the transition state for migratory insertion. The oxidative amination portion of the hydroamination reaction was calculated to be uphill by 5.9 kcal/mol, and the overall hydroamination was computed to be exergonic by 3.8 kcal/mol. These calculations strongly suggest that the combination of coordination of alkene and migratory insertion of the alkene into the Ru–N bond is irreversible and the turnover-limiting portion of this hydroamination reaction.

The results of our mechanistic investigation are summarized in Figure 7. By this mechanism, the major component of the catalyst resting state, complex **30**, is formed by coordination of the aminopyridine **1b** to the ruthenium precatalyst **Ru-1**, followed by deprotonation of the aminopyridine ligand by another molecule of **1b**. The first step of the catalytic cycle, then, involves reversible coordination of the alkene to **30** to form the alkene complex **32**. Turnover-limiting migratory insertion of the alkene into the Ru–N bond of **32** then affords the Ru–alkyl intermediate **33**, which undergoes  $\beta$ -hydride elimination to generate the hydridoruthenium enamine intermediate **45**. Subsequent exchange of the enamine for aminopyridine **1b** in intermediate **45** forms the hydridoruthenium aminopyridine intermediate **46** and free enamine **36**. Eliminated enamine **36** undergoes tautomerization to generate imine **37**, which is computed to be more stable thermodynamically than enamine **36** by 3.3 kcal/mol and would be expected to react with amine-ligated ruthenium hydride complexes by a metal–ligand bifunctional mechanism.<sup>40</sup> Thus, reduction of imine **37** by intermediate **46** affords the final hydroamination product.

The proposed catalytic cycle is supported by a large body of experimental data. The catalyst resting state **30** was identified by  $^{31}\text{P}$  NMR spectroscopy and an independent synthesis. The kinetic measurements support a mechanism by which migratory insertion of the alkene into the Ru–N bond occurs, rather than a potential nucleophilic attack on a coordinated alkene by the amine. Deuterium labeling experiments indicate that the Ru–alkyl complex **33** undergoes  $\beta$ -hydride elimination, rather than a potential direct protonation by **1b**, and hydroamination reactions conducted with added acetone imply the formation of an imine intermediate. Independent studies of the reactivity of the ruthenium–hydride complex arising from  $\beta$ -hydride elimination with the imine resulting from tautomerization of the initially formed enamine show that the reduction of the imine is much faster than the overall catalytic cycle. Finally, DFT calculations indicate that the turnover-limiting step of the reaction is migratory insertion of the alkene into a ruthenium amido complex, rather than  $\beta$ -hydride elimination from a reversibly formed insertion product.

## CONCLUSION

Ruthenium-catalyzed Markovnikov hydroamination of both unactivated and activated terminal alkenes occurs with 2-aminopyridine as a surrogate for ammonia with a stoichiometric amount of alkene by an unusual pathway for hydroamination. This process constitutes a rare example of hydroamination of alkenes with ruthenium, and it is enabled by a combination of a cationic metal center and a carefully designed aminopyridine as an ammonia surrogate. This combination facilitates the deprotonation of the aminopyridine coordinated to an electron-deficient ruthenium center, the migratory insertion of the alkene into the strained four-member ruthenacycle, and the cooperative reduction of the imine intermediate generated from  $\beta$ -hydrogen elimination to lead to an overall redox-neutral addition process. This reaction proceeds with a variety of terminal alkenes to afford the amine products under conditions with the alkene in stoichiometric quantities. A combination of experimental and computational mechanistic studies reveals that this hydroamination reaction occurs by turnover-limiting migratory insertion of the alkene into the Ru–N bond, followed by  $\beta$ -hydride elimination to generate an enamine, tautomerization of the enamine to an imine, and reduction of the imine by the hydridoruthenium aminopyridine complex to generate the amine product. This pathway implies that an enantioselective process could be developed if the step involving reduction of the imine intermediate can be rendered enantioselective. Studies to achieve such a process by this mechanism are ongoing.

## Supplementary Material

Refer to Web version on PubMed Central for supplementary material.

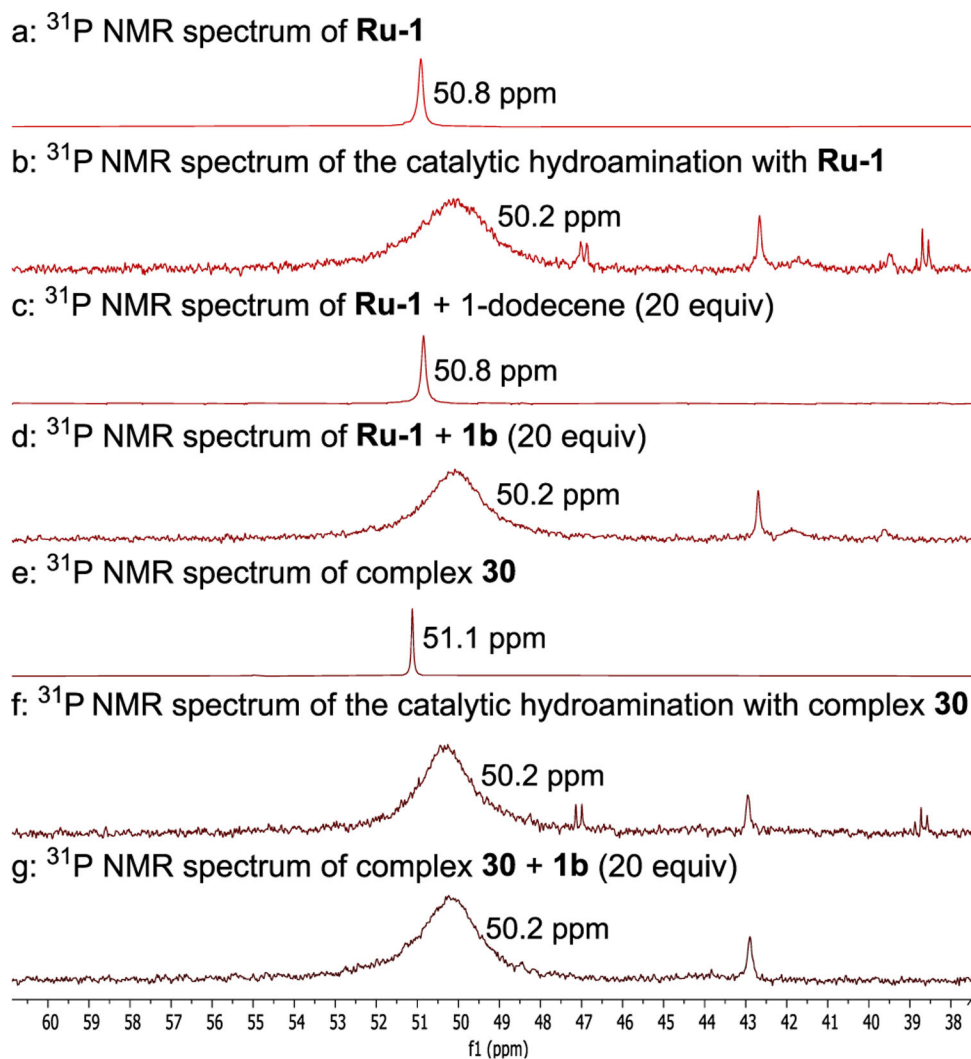
## ACKNOWLEDGMENTS

This work was supported by the NIH (R35 GM130387), the Molecular Graphics and Computation Facility at UC Berkeley (NSF CHE-0840505) for DFT calculations, and the College of Chemistry's NMR facility at UC Berkeley (NIH S10OD024998) for NMR experiments. We gratefully acknowledge Dr. Hasan Celik for assistance with NMR experiments, Dr. Nicholas Settineri for X-ray crystallography (NIH S10-RR027172), Dr. David Small and Yehao Qiu for assistance with DFT calculations, and Dr. Yumeng Xi for helpful discussions.

## REFERENCES

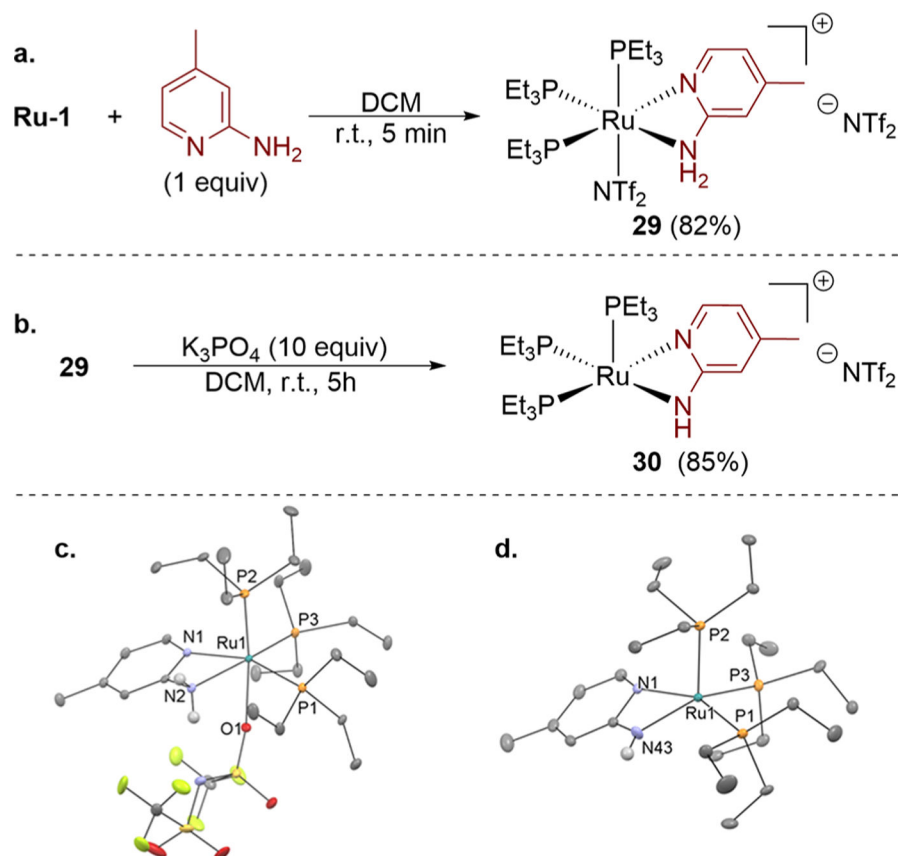
- (1). Bagley MC; Dale JW; Merritt EA; Xiong X Thiopeptide Antibiotics. *Chem. Rev* 2005, 105, 685–714. [PubMed: 15700961]
- (2). Nugent TC *Chiral Amine Synthesis: Methods, Developments and Applications*; Wiley-VCH: Weinheim, 2010.
- (3). Wang C; Bai X; Wang R; Zheng X; Ma X; Chen H; Ai Y; Bai Y; Liu Y Synthesis of Imatinib by C-N Coupling Reaction of Primary Amide and Bromo-Substituted Pyrimidine Amine. *Org. Process Res. Dev* 2019, 23, 1918–1925.
- (4). Shen Q; Hartwig JF [(CyPF-<sup>t</sup>Bu)PdCl<sub>2</sub>]: An Air-Stable, One-Component, Highly Efficient Catalyst for Amination of Heteroaryl and Aryl Halides. *Org. Lett* 2008, 10, 4109–4112. [PubMed: 18715012]
- (5). Afanasyev OI; Kuchuk E; Usanov DL; Chusov D Reductive Amination in the Synthesis of Pharmaceuticals. *Chem. Rev* 2019, 119, 11857–11911. [PubMed: 31633341]
- (6). Tripathi RP; Verma SS; Pandey J; Tiwari VK Recent Development on Catalytic Reductive Amination and Applications. *Curr. Org. Chem* 2008, 12, 1093–1115.
- (7). Müller TE; Beller M Metal-Initiated Amination of Alkenes and Alkynes. *Chem. Rev* 1998, 98, 675–704. [PubMed: 11848912]
- (8). Müller TE; Hultsch KC; Yus M; Foubelo F; Tada M Hydroamination: Direct Addition of Amines to Alkenes and Alkynes. *Chem. Rev* 2008, 108, 3795–3892. [PubMed: 18729420]
- (9). Huang L; Arndt M; Gooßen K; Heydt H; Gooßen LJ Late Transition Metal-Catalyzed Hydroamination and Hydroamidation. *Chem. Rev* 2015, 115, 2596–2697. [PubMed: 25721762]
- (10). Pawlas J; Nakao Y; Kawatsura M; Hartwig JF A General Nickel-Catalyzed Hydroamination of 1,3-Dienes by Alkylamines: Catalyst Selection, Scope, and Mechanism. *J. Am. Chem. Soc* 2002, 124, 3669–3679. [PubMed: 11929257]
- (11). Yang X-H; Lu A; Dong VM Intermolecular Hydroamination of 1,3-Dienes to Generate Homoallylic Amines. *J. Am. Chem. Soc* 2017, 139, 14049–14052. [PubMed: 28953374]
- (12). Utsunomiya M; Hartwig JF Intermolecular, Markovnikov Hydroamination of Vinylarenes with Alkylamines. *J. Am. Chem. Soc* 2003, 125, 14286–14287. [PubMed: 14624571]
- (13). Utsunomiya M; Hartwig JF Ruthenium-Catalyzed Anti-Markovnikov Hydroamination of Vinylarenes. *J. Am. Chem. Soc* 2004, 126, 2702–2703. [PubMed: 14995178]
- (14). Zhou J; Hartwig JF Intermolecular, Catalytic Asymmetric Hydroamination of Bicyclic Alkenes and Dienes in High Yield and Enantioselectivity. *J. Am. Chem. Soc* 2008, 130, 12220–12221. [PubMed: 18715004]
- (15). Dorta R; Egli P; Zürcher F; Togni A The [IrCl-(Diphosphine)]<sub>2</sub>/Fluoride System. Developing Catalytic Asymmetric Olefin Hydroamination. *J. Am. Chem. Soc* 1997, 119, 10857–10858.
- (16). Teng H-L; Luo Y; Nishiura M; Hou Z Diastereodivergent Asymmetric Carboamination/Annulation of Cyclopropenes with Aminoalkenes by Chiral Lanthanum Catalysts. *J. Am. Chem. Soc* 2017, 139, 16506–16509. [PubMed: 29117676]
- (17). Teng H-L; Luo Y; Wang B; Zhang L; Nishiura M; Hou Z Synthesis of Chiral Aminocyclopropanes by Rare-Earth-Metal-Catalyzed Cyclopropene Hydroamination. *Angew. Chem., Int. Ed* 2016, 55, 15406–15410.
- (18). Sevov CS; Zhou J; Hartwig JF Iridium-Catalyzed Intermolecular Hydroamination of Unactivated Aliphatic Alkenes with Amides and Sulfonamides. *J. Am. Chem. Soc* 2012, 134, 11960–11963. [PubMed: 22780090]
- (19). Sevov CS; Zhou J; Hartwig JF Iridium-Catalyzed, Intermolecular Hydroamination of Unactivated Alkenes with Indoles. *J. Am. Chem. Soc* 2014, 136, 3200–3207. [PubMed: 24483848]
- (20). Nguyen HN; Lee H; Audörsch S; Reznichenko AL; Nawara-Hultsch AJ; Schmidt B; Hultsch KC Asymmetric Intra- and Intermolecular Hydroamination Catalyzed by 3,3'-Bis-(trisarylsilyl)- and 3,3'-Bis(arylalkylsilyl)-Substituted Binaphtholate Rare-Earth-Metal Complexes. *Organometallics* 2018, 37, 4358–4379.

- Author Manuscript
- Author Manuscript
- Author Manuscript
- Author Manuscript
- (21). Miller DC; Ganley JM; Musacchio AJ; Sherwood TC; Ewing WR; Knowles RR Anti-Markovnikov Hydroamination of Unactivated Alkenes with Primary Alkyl Amines. *J. Am. Chem. Soc* 2019, 141, 16590–16594. [PubMed: 31603324]
  - (22). Zhang Z; Lee SD; Widenhoefer RA Intermolecular Hydroamination of Ethylene and 1-Alkenes with Cyclic Ureas Catalyzed by Achiral and Chiral Gold(I) Complexes. *J. Am. Chem. Soc* 2009, 131, 5372–5373. [PubMed: 19326908]
  - (23). Musacchio AJ; Lainhart BC; Zhang X; Naguib SG; Sherwood TC; Knowles RR Catalytic intermolecular hydroaminations of unactivated olefins with secondary alkyl amines. *Science* 2017, 355, 727. [PubMed: 28209894]
  - (24). Xi Y; Ma S; Hartwig JF Catalytic asymmetric addition of an amine N-H bond across internal alkenes. *Nature* 2020, 588, 254. [PubMed: 33142305]
  - (25). Zhang J; Yang C; He C Gold(I)-Catalyzed Intra- and Intermolecular Hydroamination of Unactivated Olefins. *J. Am. Chem. Soc* 2006, 128, 1798–1799. [PubMed: 16464072]
  - (26). Reznichenko AL; Nguyen HN; Hultsch KC Asymmetric Intermolecular Hydroamination of Unactivated Alkenes with Simple Amines. *Angew. Chem., Int. Ed* 2010, 49, 8984–8987.
  - (27). Gurak JA; Yang KS; Liu Z; Engle KM Directed, Regiocontrolled Hydroamination of Unactivated Alkenes via Protodepalladation. *J. Am. Chem. Soc* 2016, 138, 5805–5808. [PubMed: 27093112]
  - (28). Vanable EP; Kennemur JL; Joyce LA; Ruck RT; Schultz DM; Hull KL Rhodium-Catalyzed Asymmetric Hydroamination of Allyl Amines. *J. Am. Chem. Soc* 2019, 141, 739–742. [PubMed: 30614700]
  - (29). Zhu S; Buchwald SL Enantioselective CuH-Catalyzed Anti-Markovnikov Hydroamination of 1,1-Disubstituted Alkenes. *J. Am. Chem. Soc* 2014, 136, 15913–15916. [PubMed: 25339089]
  - (30). Guo S; Yang JC; Buchwald SL A Practical Electrophilic Nitrogen Source for the Synthesis of Chiral Primary Amines by Copper-Catalyzed Hydroamination. *J. Am. Chem. Soc* 2018, 140, 15976–15984. [PubMed: 30371077]
  - (31). Liu Z; Yamamichi H; Madrahimov ST; Hartwig JF Rhodium Phosphine- $\pi$ -Arene Intermediates in the Hydroamination of Alkenes. *J. Am. Chem. Soc* 2011, 133, 2772–2782. [PubMed: 21309512]
  - (32). Cheung HW; So CM; Pun KH; Zhou Z; Lau CP Hydro(trispyrazolyl)borato-Ruthenium(II) Diphosphinoamino Complex-Catalyzed Addition of  $\beta$ -Diketones to 1-Alkynes and Anti-Markovnikov Addition of Secondary Amines to Aromatic 1-Alkynes. *Adv. Synth. Catal* 2011, 353, 411–425.
  - (33). Johns AM; Sakai N; Ridder A; Hartwig JF Direct Measurement of the Thermodynamics of Vinylarene Hydroamination. *J. Am. Chem. Soc* 2006, 128, 9306–9307. [PubMed: 16848446]
  - (34). Hill CK; Hartwig JF Site-selective oxidation, amination and epimerization reactions of complex polyols enabled by transfer hydrogenation. *Nat. Chem* 2017, 9, 1213–1221. [PubMed: 29168493]
  - (35). McBee JL; Bell AT; Tilley TD Mechanistic Studies of the Hydroamination of Norbornene with Electrophilic Platinum Complexes: The Role of Proton Transfer. *J. Am. Chem. Soc* 2008, 130, 16562–16571. [PubMed: 19554728]
  - (36). Smout V; Peschiulli A; Verbeeck S; Mitchell EA; Herrebout W; Bultinck P; Vande Velde CML; Berthelot D; Meerpoel L; Maes BUW Removal of the Pyridine Directing Group from  $\alpha$ -Substituted N-(Pyridin-2-yl)piperidines Obtained via Directed Ru-Catalyzed sp<sup>3</sup> C-H Functionalization. *J. Org. Chem* 2013, 78, 9803–9814. [PubMed: 24007399]
  - (37). Ronson TO; Renders E; Van Steijvoort BF; Wang X; Wybon CCD; Prokopcová H; Meerpoel L; Maes BUW Ruthenium-Catalyzed Reductive Arylation of N-(2-Pyridinyl)amides with Isopropanol and Arylboronate Esters. *Angew. Chem., Int. Ed* 2019, 58, 482–487.
  - (38). Pan S; Endo K; Shibata T Ir(I)-Catalyzed Enantioselective Secondary sp<sup>3</sup> C-H Bond Activation of 2-(Alkylamino)pyridines with Alkenes. *Org. Lett* 2011, 13, 4692–4695. [PubMed: 21812393]
  - (39). Bruneau C; Dixneuf PH Metal Vinylidenes and Allenylidenes in Catalysis: Applications in Anti-Markovnikov Additions to Terminal Alkynes and Alkene Metathesis. *Angew. Chem., Int. Ed* 2006, 45, 2176–2203.
  - (40). Cogley CJ; Henschke JP Enantioselective Hydrogenation of Imines Using a Diverse Library of Ruthenium Dichloride-(diphosphine)(diamine) Precatalysts. *Adv. Synth. Catal* 2003, 345, 195–201.



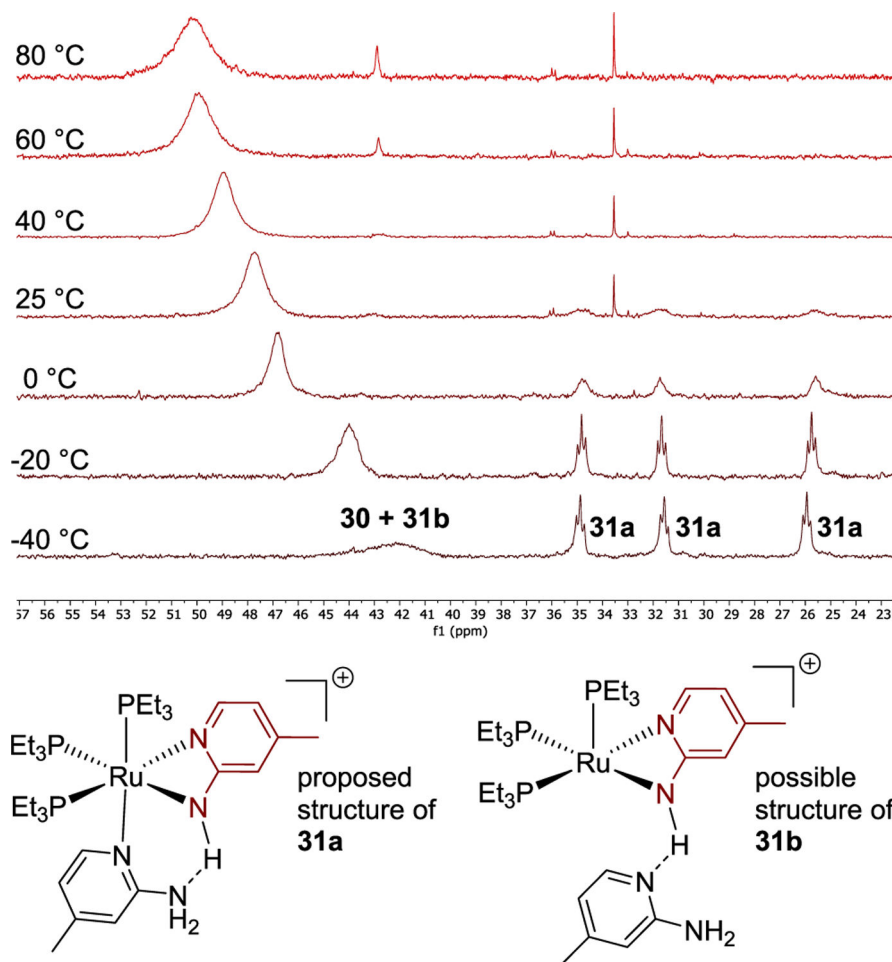
**Figure 1.** (a)  $^{31}\text{P}$  NMR spectrum **Ru-1**. (b)  $^{31}\text{P}$  NMR spectrum of the catalytic hydroamination of 1-dodecene with **Ru-1** as the catalyst. (c)  $^{31}\text{P}$  NMR spectrum of the mixture of **Ru-1** and 1-dodecene (20 equiv). (d)  $^{31}\text{P}$  NMR spectrum of the mixture of **Ru-1** and **1b** (20 equiv). (e)  $^{31}\text{P}$  NMR spectrum of complex **30**. (f)  $^{31}\text{P}$  NMR spectrum of the catalytic hydroamination of 1-dodecene with complex **30** as the catalyst. (g)  $^{31}\text{P}$  NMR spectrum of the mixture of complexes **30** and **1b** (20 equiv). All of the above spectra were acquired at 80 °C.



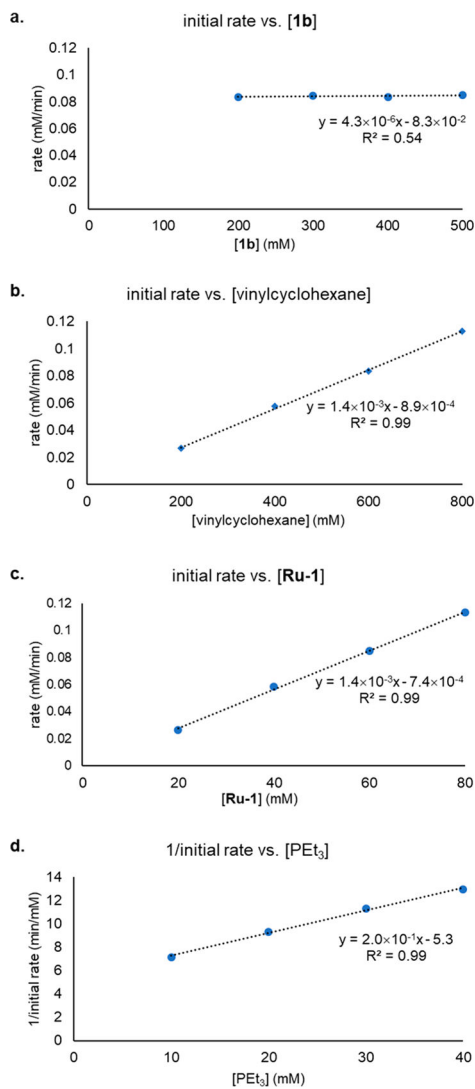
**Figure 2.**

(a) Synthesis of complex **29**. (b) Synthesis of complex **30**. (c) Solid-state structure of complex **29** with ellipsoids set at 30% and selected hydrogen atoms and free triflimide anion omitted for clarity. (d) Solid-state structure of complex **30** with ellipsoids set at 30% and selected hydrogen atoms and free triflimide anion omitted for clarity.





**Figure 3.**  $^{31}\text{P}$  NMR spectra of the mixture of complexes **30** and **1b** (20 equiv) at different temperatures and possible structures for complexes **31a** and **31b**.

**Figure 4.**

(a) Initial rates of product formation as a function of [1b]. (b) Initial rates of product formation as a function of [vinylcyclohexane]. (c) Initial rates of product formation as a function of [Ru-1]. (d) 1/initial rates of product formation as a function of [PEt<sub>3</sub>].

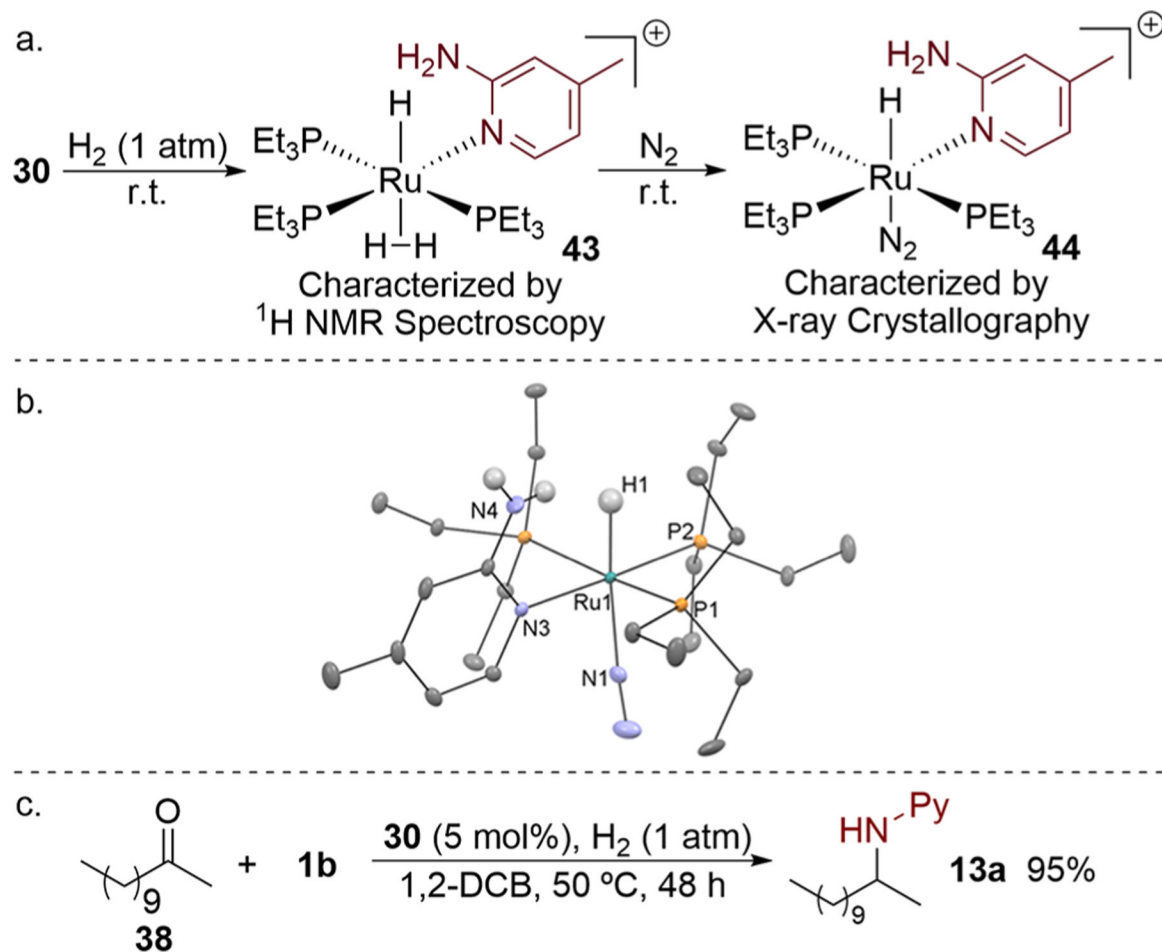


**Figure 5.** (a) Synthesis of the [Ru–H] intermediate **44**. (b) Solid-state structure of complex **44** with ellipsoids set at 30% and selected hydrogen atoms and free triflimide anion omitted for clarity. (c) Catalytic imine hydrogenation with complex **30** in the presence of  $\text{H}_2$ .

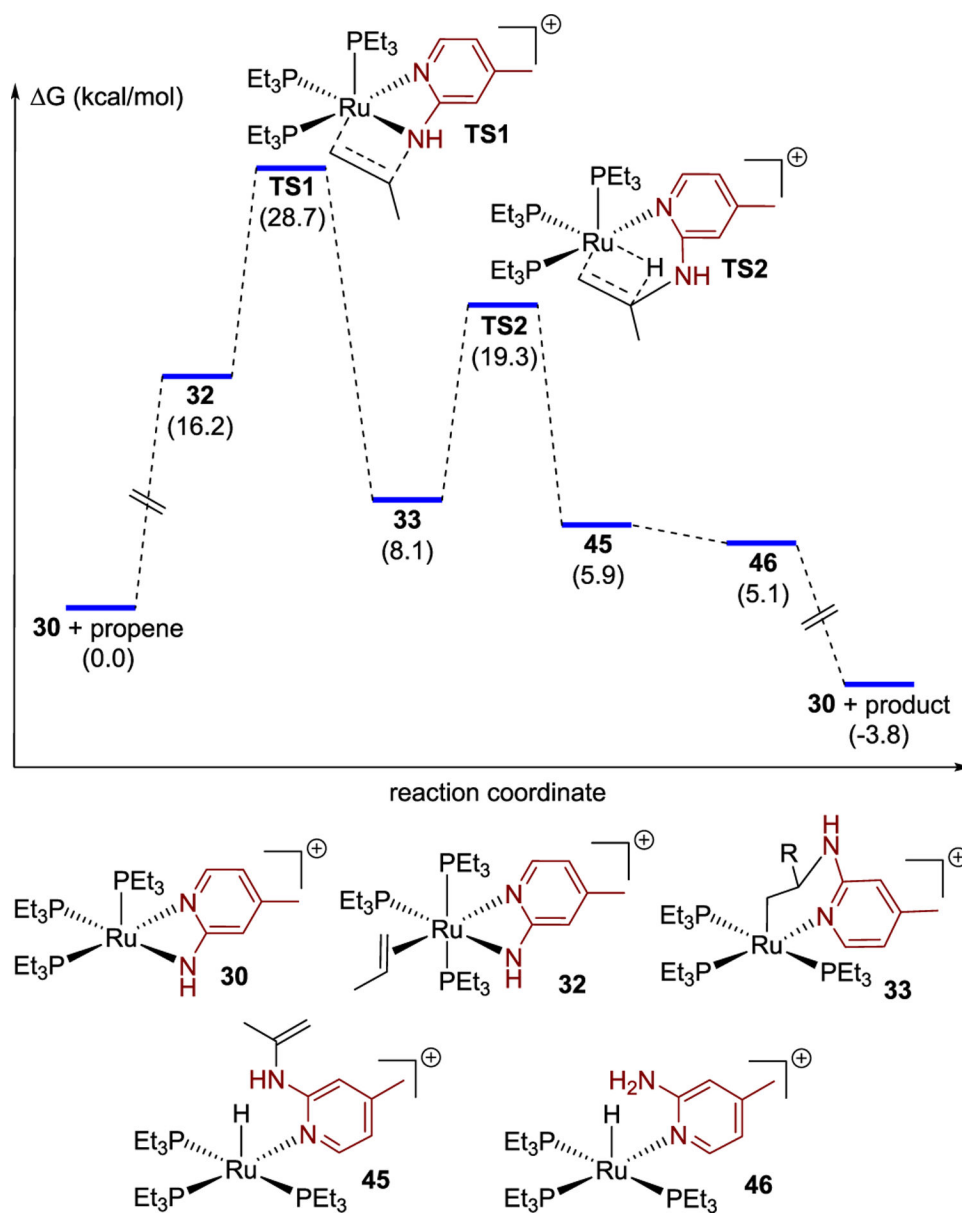


**Figure 6.** DFT computational studies on the ruthenium-catalyzed hydroamination of terminal alkenes. Free energies in kcal/mol at 80 °C are provided in parentheses.

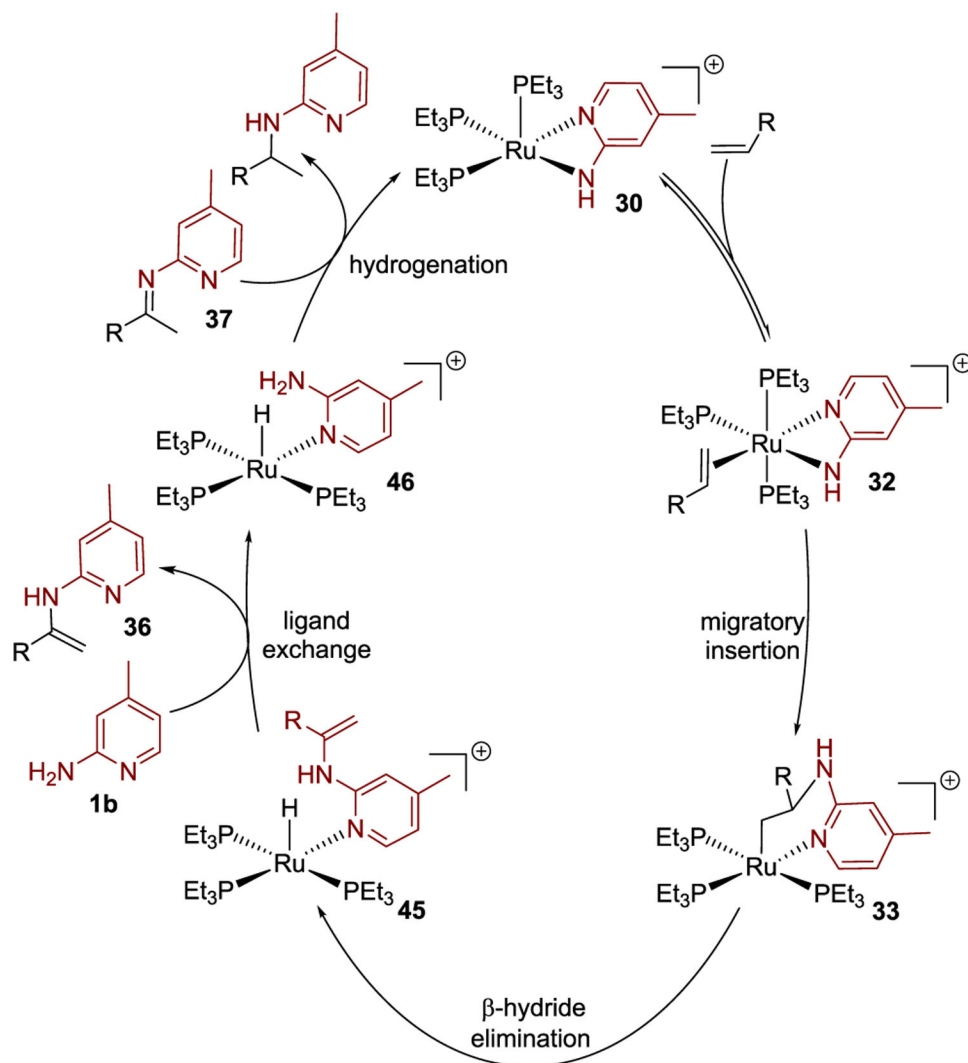
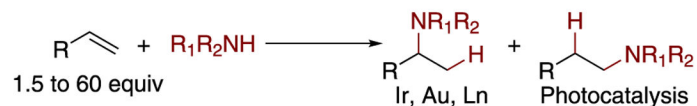
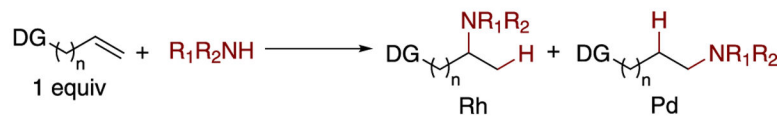


**Figure 7.** Proposed catalytic cycle for the ruthenium-catalyzed hydroamination of terminal alkenes.

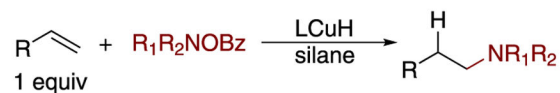
## A. Hydroamination of unactivated alkenes with large excess of alkene



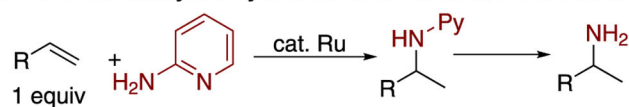
## B. Directed hydroamination of unactivated alkenes



## C. CuH-catalyzed formal hydroamination of unactivated alkenes



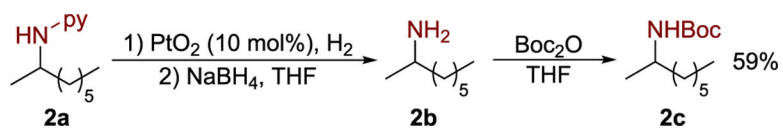
## D. This work: Ru-catalyzed hydroamination of unactivated alkenes



- Stoichiometric amount of alkene
- Alkenes with no directing group
- Unusual mechanism

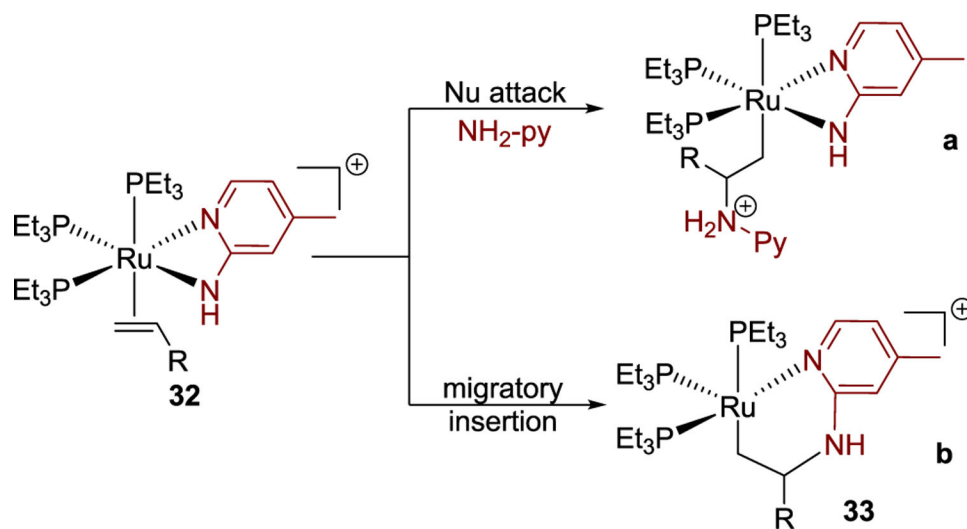
**Scheme 1.**

Catalytic Hydroamination of Unactivated Terminal Alkenes

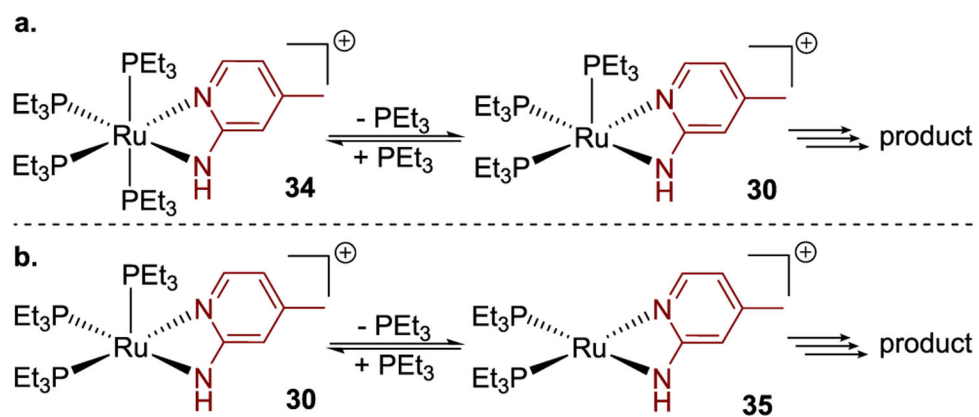


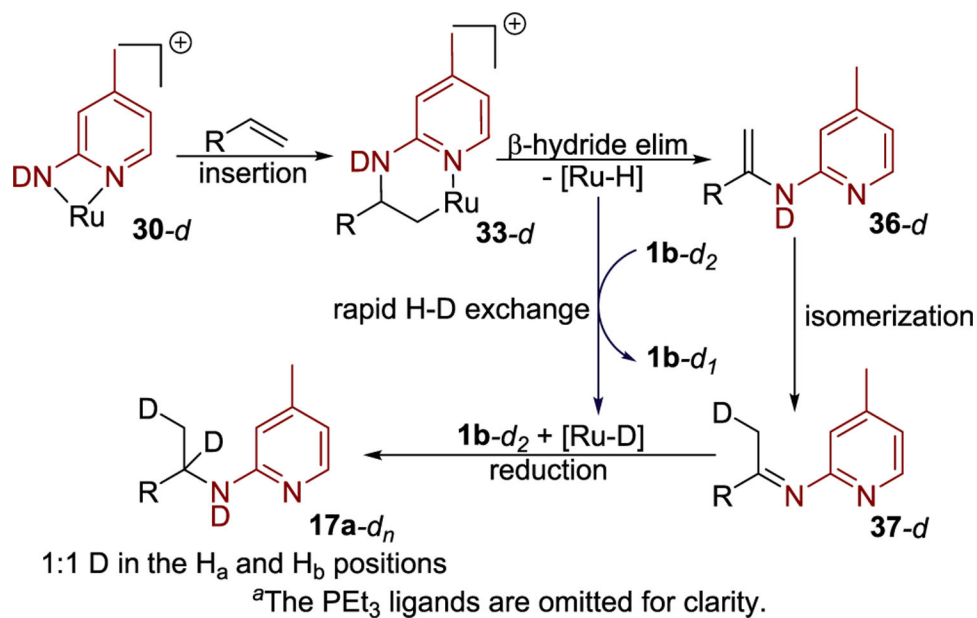
**Scheme 2.**  
Removal of the Pyridyl Group from 2a





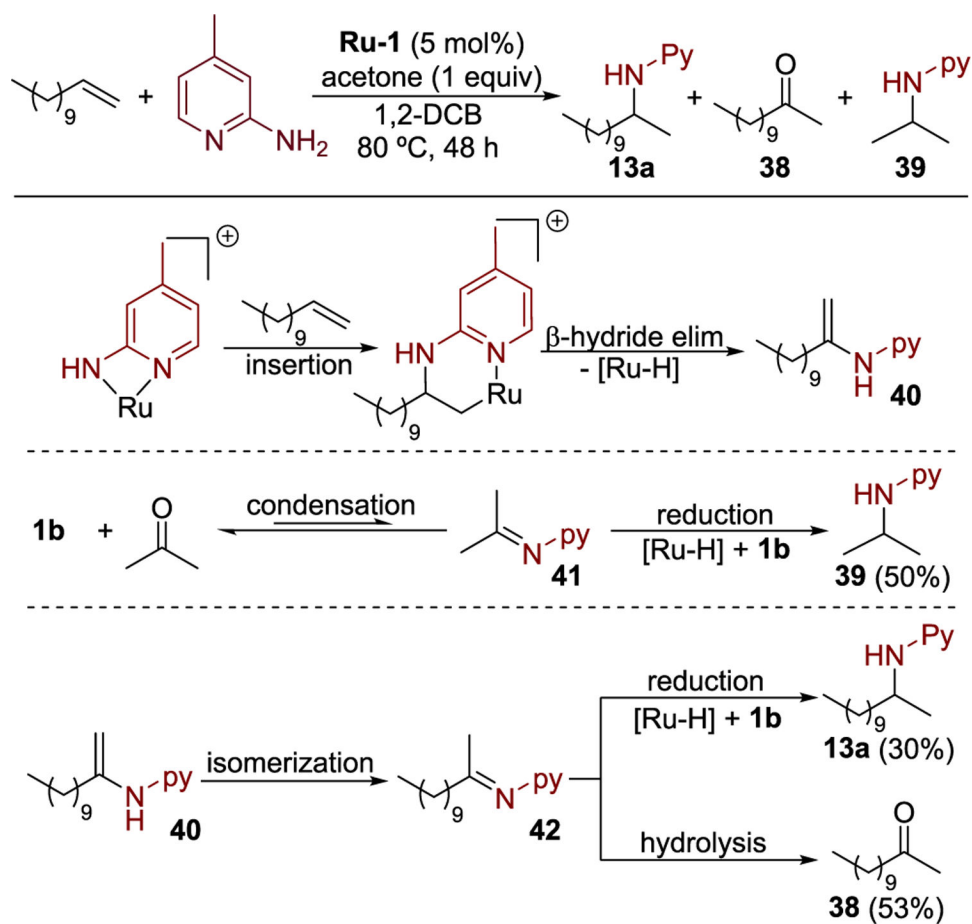
**Scheme 3.**  
Possible Pathways for the Formation of the C–N Bond





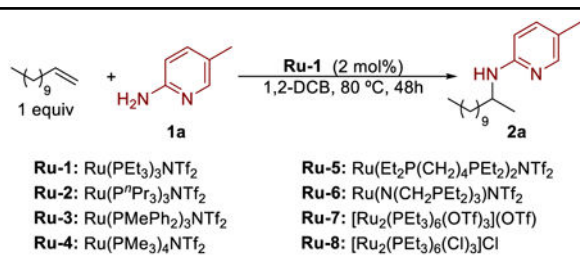
**Scheme 5. Proposed Pathway for the Formation of Hydroamination Product from 33<sup>a</sup>**

<sup>a</sup>The PEt<sub>3</sub> ligands are omitted for clarity.



**Scheme 6.**  
Hydroamination of 1-Dodecene in the Presence of Acetone

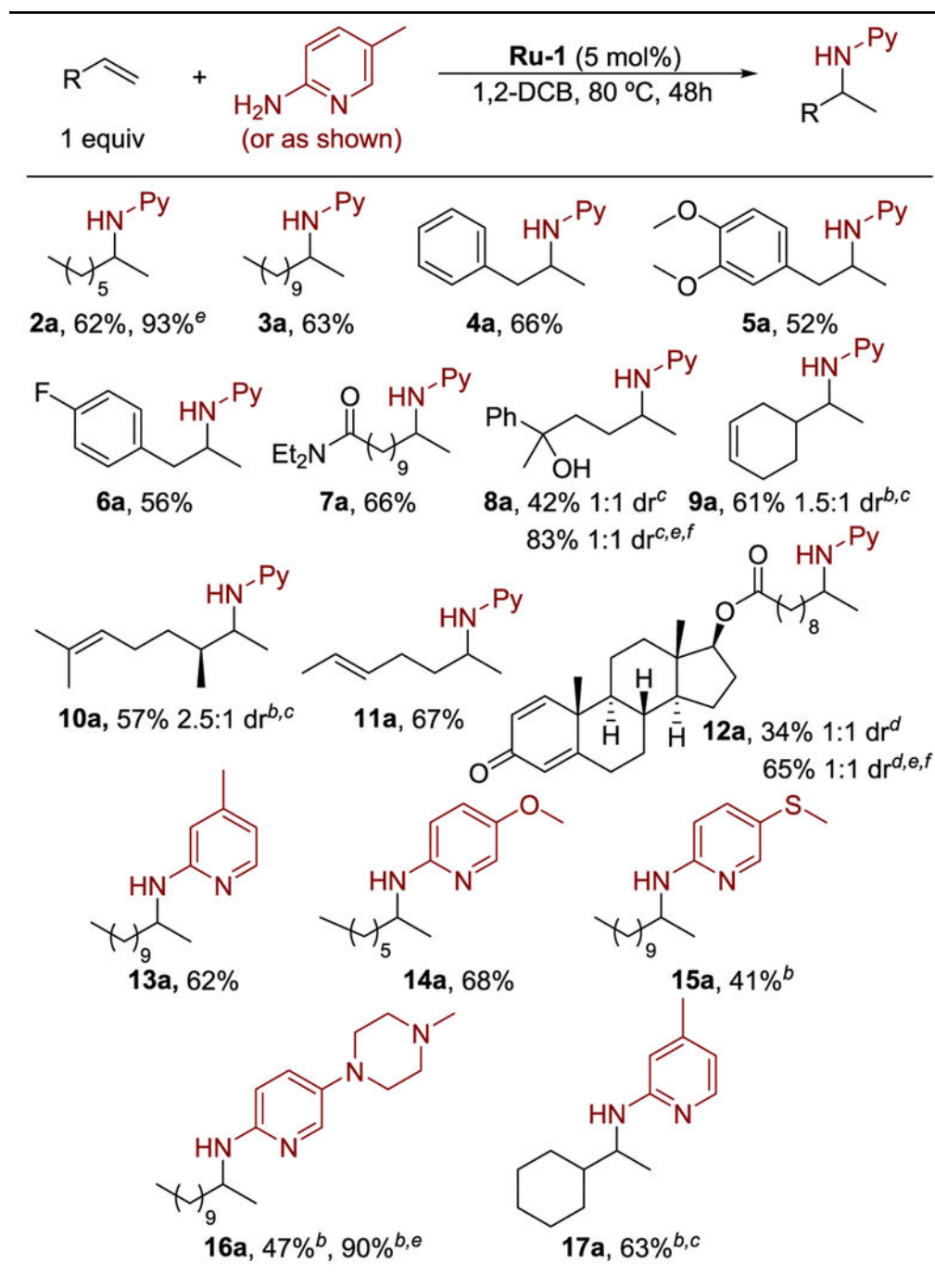
Table 1.

Evaluation of the Conditions for the Hydroamination of 1-Dodecene with **1a**<sup>a</sup>

entry	conditions	yield (%) <sup>b</sup>
1	standard	67%
2	<b>Ru-2</b> as catalyst	43%
3	<b>Ru-3</b> as catalyst	18%
4	<b>Ru-4</b> as catalyst	<1%
5	<b>Ru-5</b> as catalyst	<1%
6	<b>Ru-6</b> as catalyst	<1%
7	<b>Ru-7</b> as catalyst	62%
8	<b>Ru-8</b> as catalyst	<1%
9	1,2-DCE as solvent	<1%
10	toluene as solvent	29%
11	PhCl as solvent	48%
12	CH <sub>3</sub> CN as solvent	<1%
13	THF as solvent	56%
14	dioxane as solvent	61%
15	<b>Ru-1</b> (2 mol %)	45%
16	no <b>Ru-1</b>	<1%
17	HNTf <sub>2</sub> (5 mol %)	<1%

<sup>a</sup>Standard condition: 1-dodecene (0.2 mmol), **Ru-1** (0.01 mmol), **1a** (0.2 mmol), 1,2-DCB (50 μL), 80 °C, 48 h.<sup>b</sup>Determined by <sup>1</sup>H NMR spectroscopy of the crude reaction mixture with 1,3,5-trimethoxybenzene as the internal standard.

Table 2.

Scope of Unconjugated Alkenes and 2-Aminopyridines for Catalytic Hydroamination<sup>a,b,c,d</sup><sup>a</sup> Isolated yields.<sup>b</sup> 100 °C.

<sup>c</sup> **Ru-1** 10 mol %.

<sup>d</sup> **Ru-1** 15 mol %.

<sup>e</sup> 2 equiv of alkene.

<sup>f</sup> 72 h.

Author Manuscript

Author Manuscript

Author Manuscript

Author Manuscript



Table 3.

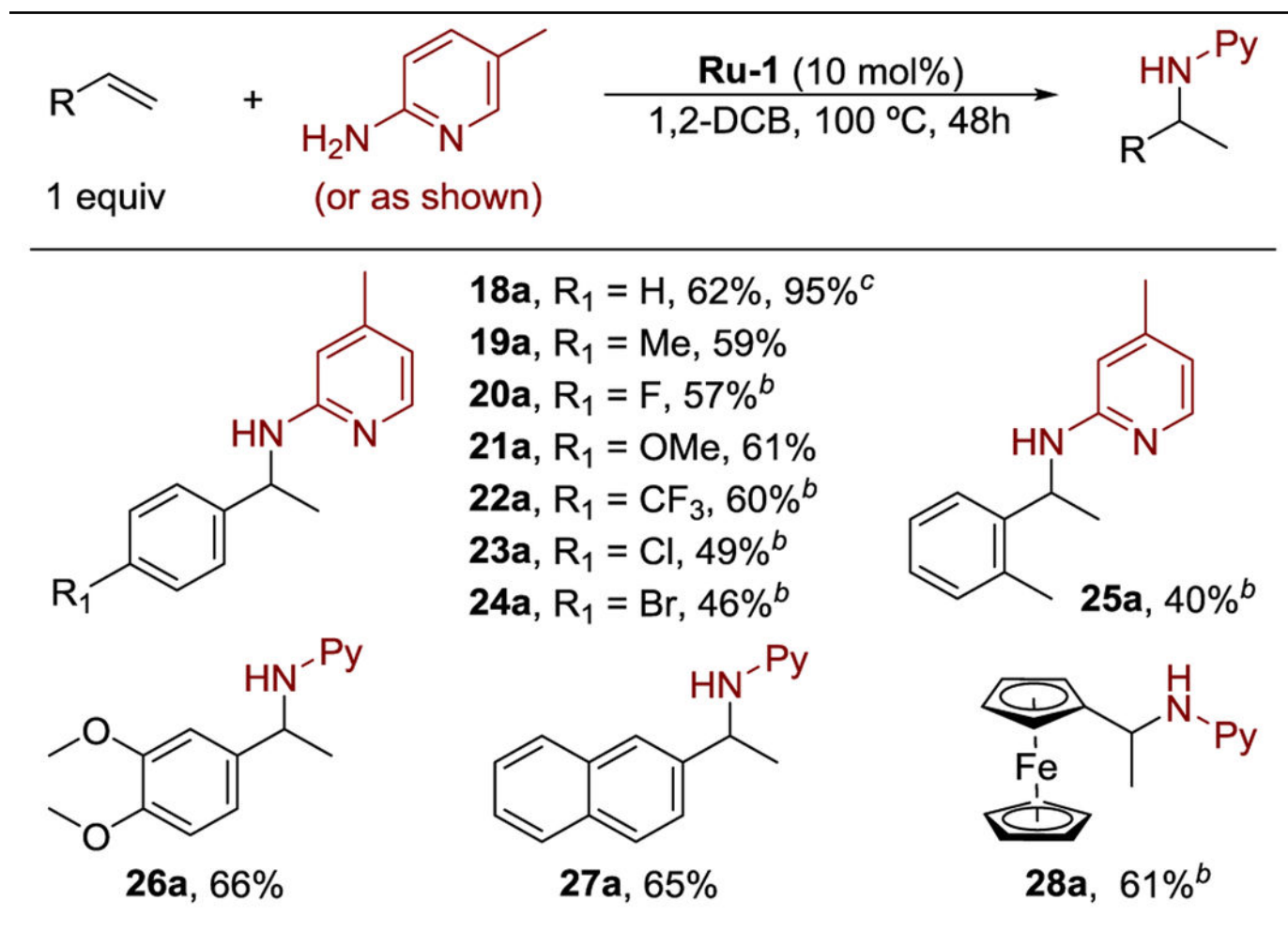
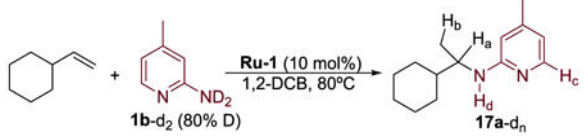
Scope of Vinylarenes for Catalytic Hydroamination<sup>a,b</sup><sup>a</sup>Isolated yields.<sup>b</sup>100 °C.<sup>c</sup>2 equiv of alkene.

Table 4.

Hydroamination of Vinylcyclohexane with 1b-d<sub>2</sub><sup>a</sup>


reaction time (h)	%D at the H <sub>a</sub> position <sup>a</sup>	%D at the H <sub>b</sub> position <sup>a</sup>
24	29%	29%
36	31%	32%
48	29%	28%

<sup>a</sup>%D incorporation = moles of D atoms/moles of product.